

## WEAK SURFACE INTERACTION IN NEMATIC LIQUID CRYSTAL – BASED COMPOSITES WITH SEMICONDUCTING NANOPARTICLES

I. ZGURA,<sup>1\*</sup> C.-P. GANEA<sup>1\*</sup>, L. NEDELICU<sup>1</sup>, C. BARTHA<sup>1</sup>, M. ENCULESCU<sup>1</sup>, L. FRUNZA<sup>1</sup>  
National Institute of Materials Physics, 405A Atomistilor Street, 077125 Magurele, Romania  
E-mails: [nedelcu@infim.ro](mailto:nedelcu@infim.ro); [cristina.bartha@infim.ro](mailto:cristina.bartha@infim.ro); [mdatcu@infim.ro](mailto:mdatcu@infim.ro); [lfrunza@infim.ro](mailto:lfrunza@infim.ro)  
\*corresponding author: [irina.zgura@infim.ro](mailto:irina.zgura@infim.ro) (I. Zgura), [paul.ganea@infim.ro](mailto:paul.ganea@infim.ro) (C.P. Ganea)

*Received*

*Abstract.* Zinc oxide (ZnO) semiconducting nanoparticles were added to a nematic liquid crystal (NLC) mixture E7, and the influence of these particles on the spectroscopic and dielectric properties of the E7 mixture was studied. ZnO nanoparticles were obtained using a recently developed green method involving clove extract. The proportion of ZnO:LC in the mixture was varied between 1:99 and 95:5% to ensure accessibility of the particle surface for interactions with LC. These natural compounds not only facilitate the formation of stable nanostructures, but also promote surface functionalization, influencing the resulting morphology, crystallinity, and dispersion behavior of the nanoparticles in the host media. Because the classical fitting models were inadequate in our systems with multiple overlapping relaxation and conduction processes, derivative-based numerical methods were employed. Such approaches enabled the resolution of up to three distinct dielectric relaxation processes and allowed the extraction of characteristic frequencies and activation energies, and insight into the underlying interfacial phenomena between the ZnO nanoparticles and LC molecules was obtained. We assumed that the interaction between the two components of the composites (NLC and ZnO) was weak, which contributes to a deeper understanding of the interplay between biofunctionalized nanostructures and anisotropic soft matter environments.

*Key words:* nematic mixture E7, confined liquid crystals, ZnO nanostructures, dielectric spectroscopy.

### 1. INTRODUCTION

Oxide-based nanomaterials have attracted growing interest in recent years due to their unique physicochemical properties, morphological versatility, and broad applicability in optoelectronics, photocatalysis, biomedical engineering, and advanced sensing technologies. Among these materials, zinc oxide (ZnO) is particularly notable for its wide direct bandgap (~3.3–3.4 eV), high exciton binding energy, strong chemical stability, and ease of synthesis in various nanostructured forms [1, 2]. Such characteristics make ZnO a versatile building block in the design of hybrid functional materials, especially in systems where tuning of the dielectric and optical properties is desired at the nanoscale.

A promising direction of current research involves the integration of ZnO nanostructures into liquid crystal (LC) matrices to create composite materials with

enhanced or tailored electro-optical behavior. These ZnO-LC hybrids benefit from the intrinsic anisotropy and dielectric responsiveness of nematic liquid crystals and the semiconducting and dipolar properties of ZnO [3, 4]. In this context, the widely used E7 nematic mixture, consisting of cyanobiphenyl and cyanoterphenyl derivatives, offers high birefringence and positive dielectric anisotropy [5], making it particularly suitable for functionalization with nano-inclusions. Interactions between nanoparticle surfaces and LC molecules may result in modified dielectric relaxation mechanisms, induced polarization effects, and altered phase transition behavior, enabling new applications in reconfigurable photonics, tunable capacitors, and sensor systems [6, 7]. Simultaneously, there has been a growing effort to align nanomaterial synthesis with green chemistry principles. The use of plant-derived extracts [8, 9, 10] as bioreductants and stabilizing agents in nanoparticle fabrication offers a sustainable and eco-friendly alternative to conventional chemical methods. In particular, extracts of *Syzygium aromaticum* (clove) have been shown to be rich in eugenol, flavonoids, and other polyphenols, which can act as both reducing and capping agents during synthesis of metals and their oxide nanoparticles [11, 12, 13]. These natural compounds not only facilitate the formation of stable nanostructures, but also promote surface functionalization, influencing the resulting morphology, crystallinity, and dispersion behavior of the nanoparticles in the host media. Based on previous experience [14], it has been suggested [15] that the formation of ZnO-NPs results from the interaction between oxygen atoms in the functional groups of clove extract and zinc from salt precursors.

In this study, we report the green synthesis of ZnO nanoparticles using aqueous clove extract, followed by their incorporation into an E7 liquid crystal matrix to form ZnO-E7 composite systems. Comprehensive characterization was performed using X-ray diffraction (XRD), scanning electron microscopy (SEM), energy-dispersive X-ray spectroscopy (EDS), and Fourier-transform infrared spectroscopy (FTIR) to confirm the structural and morphological features. Furthermore, the dielectric properties of the resulting composites were explored over a broad frequency range (0.1 Hz–10 MHz) and temperature range using broadband dielectric spectroscopy (BDS), focusing on the molecular dynamics of E7.

To address the limitations of classical fitting models such as Havriliak–Negami (HN), which are often inadequate in systems with multiple overlapping relaxation and conduction processes, we employed derivative-based numerical methods rooted in Kramers–Kronig integral relations [16, 17, 18]. These approaches enable the resolution of up to three distinct dielectric relaxation processes and allow the extraction of the characteristic frequencies and activation energies, which offers insight into the underlying interfacial phenomena between ZnO nanoparticles and LC molecules.

Overall, this study contributes to a deeper understanding of the interplay between biofunctionalized nanostructures and anisotropic soft matter environments, with

implications for future applications in adaptive, eco-sustainable electronic, and photonic devices.

## 2. Materials and Methods

### 2.1. Samples Preparation

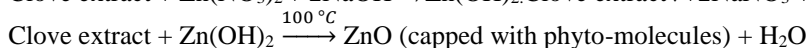
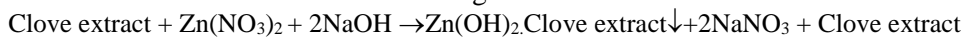
Chemical reagents  $\text{Zn}(\text{NO}_3)_2 \cdot 6\text{H}_2\text{O}$ , NaOH, and chloroform (Merck, Germany) were used without any further purification.

#### i) Preparation of clove extracts

Clove extract was prepared according to a previously shown [19]. Briefly, 10 g of the clove powder was added to 50 mL of distilled water. The suspension was boiled for 5 min, cooled to room temperature, and filtered using filter paper (Whatman filter paper no.1), resulting in an aqueous clove extract.

**ii) generation of ZnO structures** by chemical reaction between  $\text{Zn}(\text{NO}_3)_2$  and NaOH in the presence of aqueous clove extract.

The clove extract, 1:1 diluted with double-distilled water, further represented solution A. Precursors  $\text{Zn}(\text{NO}_3)_2 \cdot 6\text{H}_2\text{O}$  (0.5M) and NaOH (1M) were obtained by dissolving the corresponding compounds in distilled water (under continuous stirring), leading to solutions B and C, respectively. The latter solution was added dropwise to solution A (stirred continuously for 30 min.). The precipitate was centrifuged, washed several times to reach a neutral pH, and finally dried under vacuum at 100 °C for 2 h [19]. The obtained powder is indexed to ZnO. The synthesis of ZnO structures involves the following chemical reactions.



#### iii) obtaining E7 - ZnO composites

The E7 nematic mixture contained liquid crystals with a specific composition of 5CB: 4-cyano-4'-pentyl-1,1'-biphenyl (51 wt%), 7CB: 4-n-heptyl-4'-cyanobiphenyl (25 wt %), 8OCB: 4,4'-n-octyloxycyanobiphenyl (16 wt%), and 5CT: 4'-n-pentyl-4-cyanoterphenyl (8 wt%). This mixture of nematic LCs (NLC) has high birefringence and positive dielectric anisotropy [7].

To obtain the NLC-ZnO composite samples, suspensions were prepared by adding different amounts of ZnO to the NLC. For samples with a high concentration of ZnO ( $\geq 50\%$ ), chloroform was added as well in order to homogenize the suspension more easily. Homogeneous dispersions of NLC-ZnO were then successively ultrasonicated (Hielscher Ultrasonics, 250 W, 24 kHz) and subjected to transitions in the isotropic phase for 1 h (with a magnetic stirrer having a thermostable hob). The mixture was then drop-cast on the measuring electrode, and the sample was kept at room temperature for 24 h to remove traces of chloroform.

The samples were labelled as E7a-ZnOb, where a and b represent the mass percentages of the liquid crystal of ZnO, respectively.

### 2.2 Investigation methods

The samples were investigated structurally by X-ray diffraction (XRD) (with a Bruker D8 Advance diffractometer using  $\text{CuK}\alpha$  radiation ( $\lambda = 0.154 \text{ nm}$ ) and a Ni filter for  $\text{CuK}\beta$  morphologically and compositionally by electron microscopy (with a Zeiss Evo 50XVP instrument), optically by reflectance spectroscopy (with a Perkin Elmer Lambda 45 Uv-Vis spectrometer with an integrating sphere), and vibrationally by infrared spectroscopy (with an infrared spectrophotometer Jasco 6600 with Fourier transform). To study the thermal stability, the samples (in amount of: 4-5 mg) were measured with a SETARAM SETSYS Evolution 18 type derivatograph in TG-DSC mode. The measurements were performed in an inert atmosphere (argon) at a flow rate of 16ml / min and a heating rate of 10 °C / min.

To investigate the electrical properties of the samples as a function of frequency and temperature, the dielectric spectroscopy (DS) method was applied using an Alpha-A High Performance Frequency Analyzer together with the temperature controller QUATRO Cryosystem, from NOVOCONTROL GmbH. This method is based on the interaction between the externally applied electric field and the charge carriers in the sample. The frequency varies between 0.1 Hz and 10 MHz. The temperature varies in the temperature range in which the phase transitions of E7 occur: between 313.15 - 458.15 K /increasing the temperature with 10 K for ZnO and between 283.15 - 353.15 K / increasing the temperature with 3 K for E7-ZnO composites.

The dielectric spectroscopy (DS) experimental data were presented in the form of complex permittivity spectra. In the case of our samples, the graphical representation is difficult to analyze because of the contribution of dipolar relaxation of the constituent elements, the significant electrical conductivity resulting from the movement of free charge carriers, and their accumulation at various surfaces, which gives rise to additional relaxation mechanisms, either at the measurement cell electrodes or at the interfaces between physically distinct regions (heterogeneous phases). For this reason, we had to develop an alternative method for processing DS data, as presented in reference [18], which offers a different approach compared to the traditional method based on the use of Havriliak-Negami functions [17]. In short, it consists of the following: the processing of experimental data and obtaining reliable quantities for dielectric relaxation processes is usually performed using Havriliak-Negami (HN) functions, which contain a term of electrical conductivity [17]. HN functions are empirical but allow the analysis of a large number of sample types. The Havriliak-Negami model function encompasses several terms associated with a relaxation process and considers the contribution of electrical conductivity toward low frequencies. All parameters from the HN model functions are temperature dependent, and there are relaxation time and dielectric strength.

Dielectric spectra at certain temperatures were used to obtain the temperature dependence of all the parameters.

It is well known that the components of permittivity are linked by integral Kramers-Kronig (K-K) relations [16]. Consequently, the spectrum of the real component of the dielectric permittivity, that is, the dielectric constant, contains the same information about the dielectric relaxation processes and the spectrum of the imaginary part, that is, the dielectric loss. From an experimental point of view, there are many situations in which the electrical conductivity has values so high that it almost covers the dielectric relaxation processes at low frequencies, which makes it difficult to use the Havriliak-Negami functions. An alternative approach that significantly eliminates or diminishes the influence of electrical conductivity is the "logarithmic derivative method" [16], based on the following formula, which is a consequence of the integral relations K-K:

$$\varepsilon''_{ND}(f) = -\frac{\partial \varepsilon'}{\partial(\ln f)} \quad (1)$$

It should be noted that the calculated  $\varepsilon''_{ND}(f)$  is not entirely equal to the experimental  $\varepsilon''_{exp}(f)$ . The calculated  $\varepsilon''_{ND}(f)$  shows sharper and much better separated relaxation processes. However, the two spectra have maximum points at the same frequency values. Therefore, the characteristic frequencies were equal to each other.

Basically, the numerical derivative of the spectra of the dielectric constant  $\varepsilon'(f)$  is performed (Eq. 1). The characteristic frequencies,  $f_{max}$  are obtained from the location of the maximum points of  $\varepsilon''_{ND}(f)$ . For this purpose, we established two approaches [18]:

a) fitting with a function similar to the Cole-Cole (CC) function (Procedure I):

$$\varepsilon_{M,CC}(f) = -i \left(\frac{a}{f}\right)^N + \left(\frac{b}{1+(i \cdot f/f_{max})^m} + c\right) \quad (2)$$

where  $\varepsilon_{M,CC}(f)$  are modified Cole-Cole functions: the frequency dependence is the same, the fitting parameters  $a, N, f_{max}, b, c$ , and the exponent  $m$  might be higher than 1. We mention that the Cole-Cole function is a particular case of the Havriliak-Negami function, having a simpler analytical expression. The fitting is performed by minimization of the following expression:  $\sum_j [\varepsilon_{M,CC}(f_j) - \varepsilon''_{ND}(f_j)]^2$

b) Calculate the second logarithmic derivative and find the maximum point,  $f_{max}$ , from the graphic solution of the equation (Procedure II):

$$\frac{\partial \varepsilon''_{ND}}{\partial(\ln f)} = -\frac{\partial^2 \varepsilon'}{\partial(\ln f)^2} = 0 \quad (3)$$

Once the  $f_{max}$  value for the temperature corresponding to each permittivity spectra is established, we can proceed to the next step: The activation energy  $E_A$  is obtained by graphical Arrhenius-type representation of  $\ln f_{max}$  as a function of  $1000/T$ , followed by the fit with the Arrhenius function:

$$\ln f_{max} = \ln f_{\infty} - \frac{E_A}{1000 \cdot k_B} \cdot \frac{1000}{T} \quad (4)$$

### 3. Results and Discussion

The diffractogram of the ZnO sample (Fig. 1a) reveals two  $\theta$  maxima at 31.8 °, 34.7 °, 36.3 °, 47.6 °, 56.6 °, 62.9 °, 66.4 °, 67.9 °, and 69.1 °, corresponding to the Miller indices of the (100), (002), (101), (102), (110), (103), (200), (112), and (201) planes, respectively. All the observed diffraction maxima were assigned to ZnO in the hexagonal phase of wurtzite (JCPDS no. 01-082-9745), confirming the formation of ZnO.

The SEM image (Fig. 1b) shows spherical ZnO particles (average size ~ 100 nm). EDS mapping (Fig. 2) shows the distribution of O, Zn, and C, and the elemental maps confirm the presence of ZnO in the investigated sample.

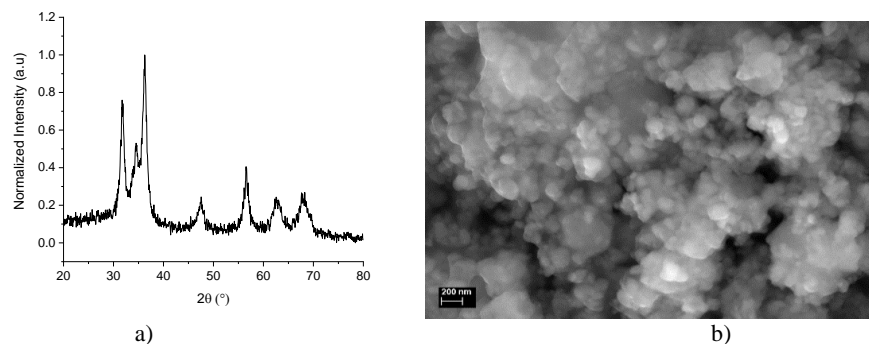


Fig. 1 - (a) XRD pattern and (b) SEM image of ZnO structures

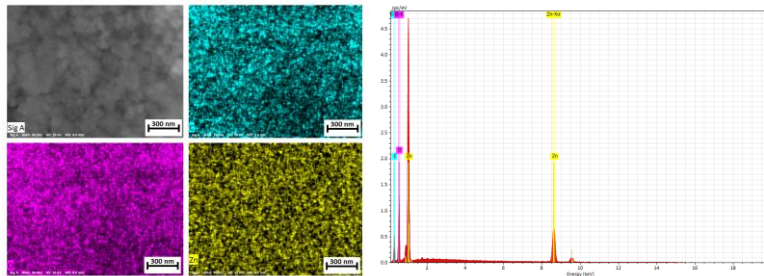


Fig. 2. - EDS mapping with the distribution of O, Zn and C elements.

Based on the reflection spectroscopy data, the Kubelka-Munk function ( $f(R) = (1 - R)^{1/2}/2R$ ) was represented graphically (Fig. 3), from which the value of the band gap of ZnO was estimated at ~ 3.3 eV, in accordance with the data reported in the literature for different morphologies of ZnO (e.g., for nanowires obtained by thermal oxidation [2] or hydrothermally [20]). The FTIR spectra of pure ZnO (Fig. 4, blue curve) and the E7-ZnO composites highlight the ZnO-specific band at 455  $\text{cm}^{-1}$  [19]. Additionally, broad peaks in the OH stretching region (ca. 3400-4000  $\text{cm}^{-1}$ ) are also present in all spectra (Fig. 4), indicating the existence of an OH surface layer and/or adsorbed water [21, 22].

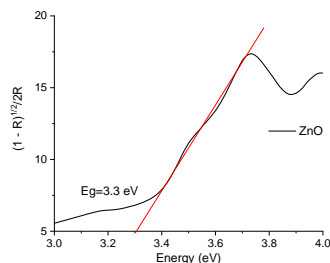


Fig. 3 - Kubelka-Munk function of the pristine ZnO sample;

The interaction of NLC molecules with the surface of ZnO particles was also investigated by FTIR, see Fig. 4, the red and green curves. One can observe the absorption peaks arising from the vibrations of different functional groups in the NLC molecules. Thus, we see peaks in the region of CH stretching, CN stretching, out-of-plane ring vibrations, CC ring stretching, CH<sub>n</sub> deformation, etc. [23], in decreasing order of their position (given in wavenumbers). The composite peaks were correlated with those of the pure materials. In the composite samples, the positions of the peaks related to LC, especially those from 2226 cm<sup>-1</sup> [24, 25] associated with the CN stretching vibration, are not modified, which indicates that the peaks have bulk-like behavior (without the components of the interaction surface layer). This is shown in Fig. 5. too.

In fact, it was shown that ZnO particles can interact with cyanobiphenyls [26], showing an improvement in the alignment of the liquid crystal with increasing weight percentage of ZnO nanoparticles, from *ca.* 1% up to a concentration of 30 wt %. A different behavior as observed in our case might be explained supposing ZnO surface was capped by cloves compounds. Composite peaks are complex and can be decomposed into Gaussians attributed to different species such as (in the order of decreasing wavenumber) dimer [27] and monomer bulk-like species around 2226 cm<sup>-1</sup>, tilted species appearing at *ca.* 2230 cm<sup>-1</sup> [28, 29]; species absorbing at wavenumbers greater than 2230 cm<sup>-1</sup> are those interacting with the hydroxyl groups on the surface of the host by hydrogen bonds, or species coordinately bonded to Lewis acid ions absorbing at around 2270 cm<sup>-1</sup> [30]. Although the deconvolution procedure of the IR absorption peaks might allow the estimation of the area under the peaks belonging to different components, such a comparison is difficult in our case because of the incertitude of deconvolution.

The most sensitive peak to the environment is due to the stretching of the CN bond, the position of which is significantly influenced by NLC bonding to the particle surface. Fig. 5 shows the peaks in the corresponding stretching regions and their deconvolution into Gaussians. Two samples were chosen for discussion: bulk E7 and a composite with a few E7, which can be distributed onto the ZnO surface.

The CN stretching peak has the same position (at  $2226\text{ cm}^{-1}$ ) in the two considered samples and almost the same bandwidth ( $10.2$  and  $9.4\text{ cm}^{-1}$  respectively).

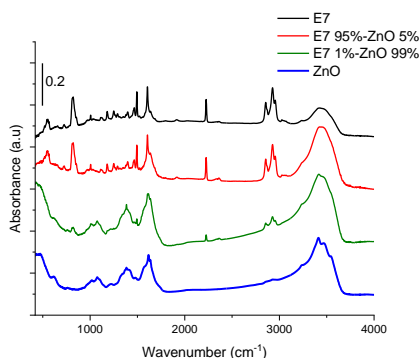


Fig. 4 - FTIR spectra corresponding to the samples as shown in the legend. The spectra have been shifted vertically to make them easier to see.

The region of out-of-plane vibration is also very sensitive to the interaction of the benzene ring CH bonds with the oxide surface. In Fig. 5 b) and b'), peaks appear in this region for the same samples as in Fig. 5 a) and a'). The peaks appearing in the case of E7 were positioned at ca.  $1800\text{ cm}^{-1}$  and  $1916\text{ cm}^{-1}$ . These vibrations in the composite appear at the same position as for bulk E7; we stress that the small peaks in Fig. 5b' are artifacts.

Weight loss due to the burning and decomposition of organic molecules was investigated by DSC-TG measurements. The TG curves of the ZnO samples are shown in Fig. 6 ( $20 - 800\text{ }^{\circ}\text{C}$ ), with total percentage of weight loss of 16%. The initial weight loss ( $\sim 3\%$ ) observed below  $200\text{ }^{\circ}\text{C}$  corresponded to the loss of water adsorbed on the sample surface. The range  $400-500\text{ }^{\circ}\text{C}$  corresponds to the release of inorganic compounds from the sample (approximately 3%). In the final stage (range  $700-800\text{ }^{\circ}\text{C}$ ), the weight loss of the sample is very small (approximately 1%). In the DGA analysis, there was an exothermic peak that could indicate the presence of a small amount of organic material [31]. In the case of the E71%-ZnO99% sample, the TG analysis revealed that the total percentage of mass loss was 7%, whereas for the E795%-ZnO5% the mass loss was 79% at  $800\text{ }^{\circ}\text{C}$ . This result can be explained by considering the thermal stability of ZnO and the compositions of the samples. The DGA representation shows an exothermic peak, indicating the presence of organic material (E7). Previous thermogravimetric investigations of related composites of 8CB and Aerosil [32] have shown that at least three and possibly more weight loss processes seem to occur under the aforementioned experimental conditions because shoulders or asymmetric loss curves might hide others.

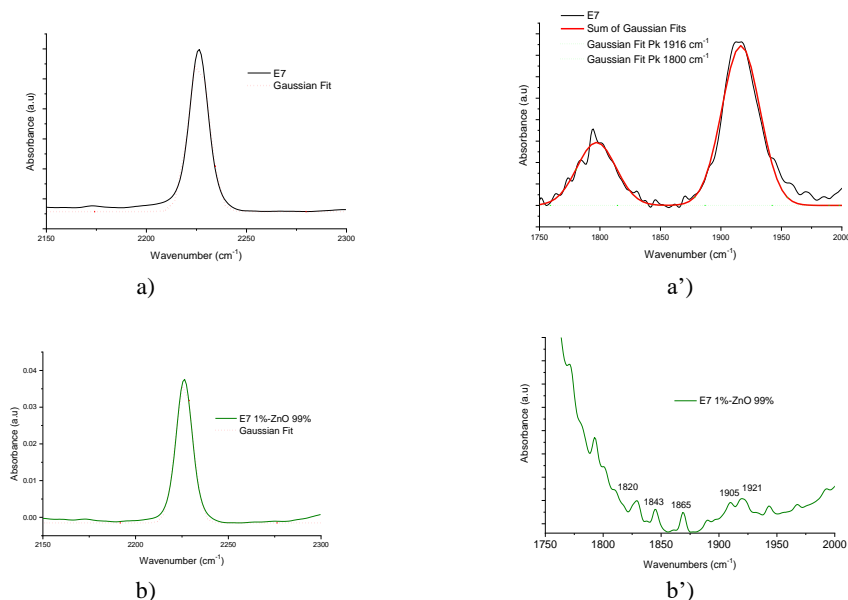


Fig. 5 - Decomposition using Gaussians (dot-dashed lines) of the -CN stretching vibration spectrum and the spectrum in the range of out-of-plane vibration for a) and a') E7 liquid crystal; b) and b') sample E7 1%/ZnO 99%.

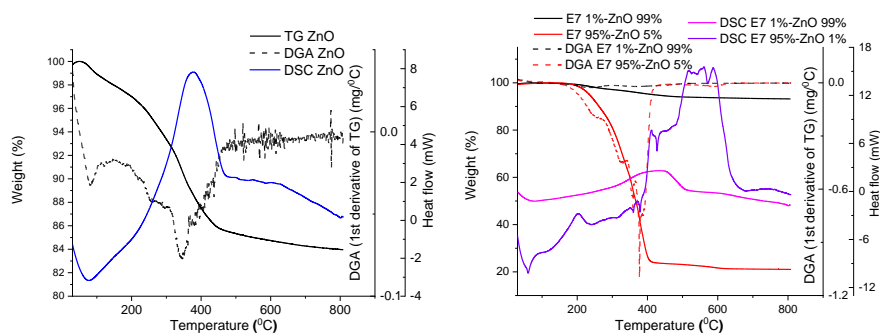


Fig. 6 - TG, DGA and DSC curves of the selected samples

The main DTG peaks at ca. 640 and 840 K shifted toward lower and higher temperatures, respectively. The same tendency can also be observed in the present cases, but the shift is smaller, which can be explained by a weak interaction with the surface. Fig. 7 shows the induced changes in the electrical properties of the two pure components (E7 and ZnO) and the E7-ZnO composites (at different mass ratios between the two components) with frequency and temperature. For a more suggestive presentation, the chosen electrical quantities were the components of the permittivity, the real part,  $\epsilon'(\omega)$ , called the dielectric constant, and the imaginary part,  $\epsilon''(\omega)$ , called the dielectric loss, and the real part of the electrical conductivity,

$\sigma'(\omega)$ . To form a more complete picture of the electrical property behavior, we considered it necessary to represent all these quantities as functions of frequency and temperature. In this figure, the spectra of the electrical conductivity and dielectric losses are presented to emphasize the effects of the different conduction and/or dielectric relaxation mechanisms. In addition, it can be seen that the dielectric loss presents a maximum toward high frequencies, and the conductivity shows an extended plateau over several decades in the middle of the frequency domain. The plateau width decreased with increasing ZnO concentration. The ZnO sample did not exhibit this plateau. Moreover, for this sample, the shapes of the spectra differ from those of the composites, especially for dielectric losses; ZnO samples exhibit a non-monotonous variation with the temperature of all electrical quantities. Thus, there is an increase in the dielectric loss at relatively low temperatures, reaching a maximum, followed by a decrease to a minimum in the region of average temperatures. At high temperatures, the dielectric loss also increased. The conductivity exhibits the same variation as the dielectric loss. With the addition of ZnO nanoparticles, the conductivity decreased.

The presence of the plateau in the medium-frequency domain indicates an important component of the electrical conductivity owing to the free charge carriers. The additional decrease in conductivity at lower frequencies can be determined by the Maxwell-Wagner (M-W) effect or electrode polarization (EP) effects. In this frequency domain, a small but noticeable change was observed in the slope of the dielectric loss  $\varepsilon''(\omega)$ . The slope changed from one value to another at frequencies between 10 Hz and 100 Hz. The increase of the dielectric losses at low frequencies by several orders of magnitude is due to the conductivity and/or dielectric relaxation processes mentioned above. The two possible mechanisms are masked by the high electrical conductivity. To analyze the spectra in which the conductivity has high values, it is necessary to use the derivative method with the logarithm of the frequency of the dielectric constant [16].

The spectra of the electrical quantities varied significantly with the ZnO concentration. To establish a correspondence between the composition and electrical properties, we obtained information regarding the quantities that describe the mechanisms at the molecular scale, that is, dipolar relaxation.

### **Processing and interpretation of DS data**

ZnO is an n-type semiconductor with a wide bandgap (3.37 eV). Its electrical conductivity is due to the excess zinc placed in interstitial positions [1, 33] and oxygen vacancies [34]. ZnO is characterized by a wurtzite-type crystalline structure, which causes the ZnO particles to have a permanent dipole electric moment. ZnO particles also exhibit orientational polarization. Experimentally, it was observed that the value of the dipole electric moment depends on the volume and on the dimensions of the micro/nanoparticle [3].

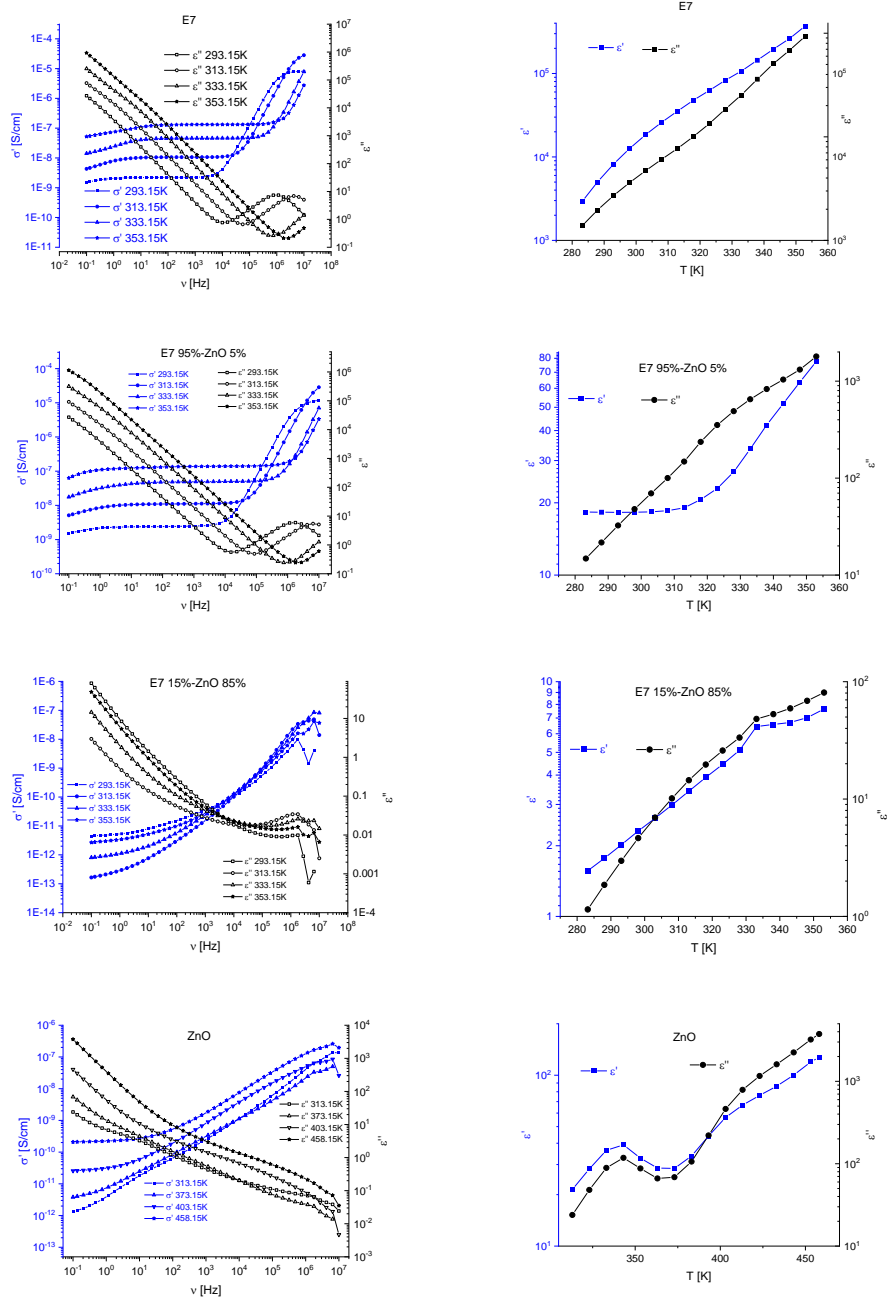


Fig. 7 - Spectra of electrical quantities (left) and their temperature dependence at a certain frequency (right) for pure E7, ZnO, and E7-ZnO composite samples

Nematic liquid crystal E7 (NLC) has been intensively studied [5], and its electrical properties (dielectric permittivity, dielectric loss, and electrical conductivity) can be modified by doping with micro/nanoparticles of ZnO through interactions such as inorganic particle-inorganic particles, inorganic particle-NLC molecules, and NLC molecule-surface electrodes, against the background of the NLC-NLC molecular dipole interaction [4]. However, the concentration of micro/nanoparticles changes the number of ionic impurities introduced by doping, resulting in a change in electrical conduction. Thus, an important parameter is the characteristic time or frequency of the dielectric relaxation processes owing to the interactions between the two components (ZnO and E7). Because the volume of experimental data and numerical processing is very large, we briefly present what we found and summarize the final results obtained based on numerical analysis as follows. The conclusions presented below are based on the dielectric spectral analysis method developed in our previous study [18].

The  $\varepsilon''_{ND}(f)$  spectra of the E7-ZnO composites have three relaxation processes (low-frequency, medium-frequency, and high-frequency). The dielectric relaxation at high frequencies originates from the dipolar relaxation of liquid crystal molecules. This shows how the liquid crystal interacts with ZnO nanoparticles in the case of the composite samples. Hence, to analyze the HF-relaxation process (based on Procedure I), Fig. 8a presents the dependence of the activation energy on the sample EA, which is between 0.675 eV (58.567 kJ/mol) and 0.607 eV (65.128 kJ/mol). There was a tendency to increase the characteristic frequency with a decrease in the NLC concentration and a decrease in the activation energy with an increase in the NLC concentration. The activation energy values were compared with those determined for composites containing nCBs and Aerosil [6].

The estimated activation energies are rather high ( $E_A < 60\text{--}65 \text{ kJ mol}^{-1}$ ) and the pre-factors are between  $10^{15}$  and  $10^{17}$  Hz. These values are related to the interaction of the LC molecules with the silica surface, which also slows down the molecular dynamics. The values found in the case of ZnO nanoparticles can be even smaller than those in the case of aerosil. Fig. 8b presents the concentration dependence of the activation energy using numerical calculation of the dielectric constant derivative, Procedure II. The concentration dependence of the activation energy has a more irregular shape, most likely due to high errors occurring at high frequencies because of the measurement of the phase shift and errors arising from the numerical calculation of the dielectric constant derivative.

The differences between the processing results obtained using these methods were very small. So, the use of the two numerical methods to obtain the characteristic frequency has shown that the methods verified each other.

Fig. 8 (a and b) show some similarities, a tendency to increase the activation energy and characteristic frequency with increasing ZnO concentration.

The two quantities ( $\ln f_{max}(1/T)$ ,  $E_A$ ) obtained by both numerical methods [18] were relatively close. The dependence of the activation energy on ZnO concentration

is an interesting finding, although such a dependence was observed in the literature for other systems [35].

The results show a low-intensity interaction between the two components of the composite samples (liquid crystal and nanoparticles). This conclusion is consistent with the FTIR measurements.

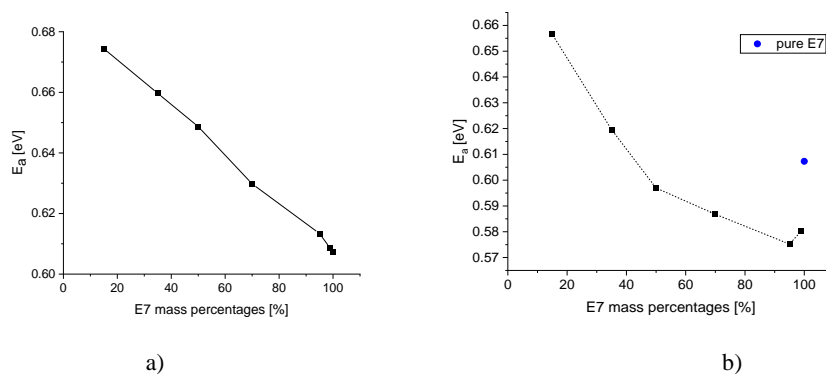


Fig. 8. a) dependence of the activation energy on the sample composition-Procedure I; b) dependence of the activation energy on the sample concentration in E7-Procedure II.

## 5. Conclusions

The ZnO powder was synthesized using a wet chemical method. The X-ray diffraction and EDS mapping show that the synthesized composites contain only ZnO (indexed to hexagonal wurtzite phase, having only in composition the O, Zn and C elements) with a value of the band gap estimated at  $\sim 3.3$  eV, from UV-Vis reflection data. The SEM images revealed that ZnO was formed by agglomerated nanoparticles with an average size of approximately 100 nm. From FTIR measurements, we can conclude that the LC maxima located at 2226  $\text{cm}^{-1}$ , associated with the CN stretching vibration, were not modified, suggesting a bulk-like behavior of the liquid crystal in the composite samples.

The shape of the dielectric spectra made it necessary to renounce the analysis based on HN functions. As an alternative, we used two numerical procedures that were deduced using the logarithmic derivative as the primary starting point. The developed numerical methods led to consistent and conclusive results, where the activation energy slightly increased with increasing ZnO concentration in the composites. The variations are small enough, so we can say about a weak interaction between the two components of the composite samples (NLC and ZnO). This conclusion was consistent with the FTIR results.

*Acknowledgements.* This work was supported by a grant from the Ministry of Research, Innovation and Digitization, CNCS/CCCDI—UEFISCDI, project number COFUND-WATER4ALL-WATER Green Treat-1, No. 59/2024, within PNCDI IV, and project number

PN-III-P4-PCE-2021-1131, within PNCDI III. The authors thank Nicoleta Preda for valuable suggestions regarding the interaction between ZnO and the organic medium.

#### REFERENCES

1. P.P. Sharmila, N.J. Tharayil, AIP Conf. Proc., 1620, 462 (2014)
2. C. Florica, N. Preda, A. Costas, I. Zgura, I. Enculescu, Mater. Lett., 2016, 170, 156–159.
3. L. S. Li, Y. J. Huang, J. Phys. D: Appl. Phys., **42**, 125413 (2009)
4. P. K. Tripathi, A. Kr. Misra, S. Manohar, S.Kr. Gupta, R. Manohar, J. Mol. Struct., **1035**, 371–377 (2013).
5. M.T. Viciosa, A. M. Nunes, A. Fernandes, P.L. Almeida, M. H. Godinho, M. D. Dionísio, Liq. Cryst., **29**, 429–441 (2002).
6. S. Frunza, L. Frunza, M. Tintaru, I. Enache, T. Beica, A. Schoenhals, Liq. Cryst. **31**, 913–922 (2004).
7. P. Porov, V.S. Chandel, Trans. Electr. Electron. Mater., **17**, 69–78 (2016).
8. J. Singh, T. Dutta, K.H. Kim, M. Rawat, P. Samddar, P. Kumar, J. Nanobiotechnology, **16**, 84 (2018).
9. M. Ramesh, M. Anbuvarannan, G. Viruthagiri, Spectrochim. Acta A, **136**, 864–870 (2015).
10. S. Ahmed, M. Ahmad, B.L. Swami, S. Ikram, J. Radiat. Res. Appl. Sci., **9**, 1–7 (2016).
11. K. Haiouani, S. Hegazy, H. Alsaeedi, M. Bechelany, A. Barhoum, Materials **17**, 4340 (2024).
12. N. A. Hussien, M. A. E.F. Khalil, M. Schagerl, S. S. Ali, Int J Nanomedicine. **20**, 4299–4317 (2025).
13. F. HajiSadeghi, A. N. Nasab, S. Rashki, H. Zandi, S. Afsharikhah, Z. S. Fatemi-Nasab, A. Nazari-Alam, The Microbe, **7**, 100363 (2025)
14. E.F. El-Belily, M.M.S. Farag, H. A Said, A.S. Amin, E. Azab, A.A. Gobouri, A. Fouda, Nanomaterials **11**, 95 (2021).
15. S. Azizi, F. Namvar, M. Mahdavi, M. B. Ahmad, R. Mohamad, Materials **6**, 5942–5950 (2013).
16. F. Kremer, A. Schönhal (Eds.), Broadband Dielectric Spectroscopy, Springer, Berlin, 2003.
17. S. Havriliak, S. Negami, Polymer, **8**, 161–210 (1967).
18. C.P. Ganea, I. Zgura, L. Frunza, Mater. Chem. Phys., **309**, 128372 (2023).
19. I. Zgura, M. Enculescu, C. Istrate, R. Negrea, M. Bacalum, L. Nedelcu, M.E. Barbinta-Patrascu, Nanomaterials **10**, 2146 (2020).
20. L. V. Podrezova, S. Porro, V. Cauda, M. Fontana, G. Cicero, Appl. Phys. A **113**, 623–632 (2013).
21. A. Önsten, D. Stoltz, P. Palmgren, S. Yu, M. Göthelid, U. O. Karlsson, J. Phys. Chem. C **114**, 11157–11161 (2010).
22. M. Iachella, J. Cure, M. D. Rouhani, Y. Chabal, C. Rossi, A. Estève, J. Phys. Chem. C **122**, 21861–21873 (2018).
23. L. Frunza, I. Zgura, C. P. Ganea, V. A. Loiko, D. Manaila-Maximean, Liq. Cryst., **50**, 1169–1176 (2023).
24. K. Ha, J. L. West, Liq. Cryst. **31**, 753 (2004).

25. A. R. Brás, S. Frunza, L. Guerreiro, I. M. Fonseca, A. Corma, L. Frunza, M. Dionísio, A. Schönhals, *J. Chem. Phys.* **132**, 224508 (2010).
26. L. J. Martínez-Miranda, K. M. Traister, I. Meléndez-Rodríguez, L. Salamanca-Riba, *Appl. Phys. Lett.* **97**, 223301 (2010),
27. G. A. Puchkovskaya, A. Yu. Reznikov, A. A. Yakubov, O. V. Yaroshchuk, A. V. Glushchenko, *J. Mol. Struct.* **381**, 133 (1996).
28. Y. W. Zhou, M. Jaroniec, R. K. Gilpin, *Anal. Chem.* **66**, 4100 (1994)
29. Y. W. Zhou, M. Jaroniec, G.L. Hann, R. K. Gilpin, *Anal. Chem.* **66**, 1454 (1994).
30. L. Frunza, H. Kosslick, U. Bentrup, I. Pitsch, R. Fricke, S. Frunza, A. Schönhals, *J. Molec. Struct.* **341**, 651-653 (2003).
31. N. Jayarambabu, B. Sivakumari, Y. T. Prabhu, *Int. J. Curr Eng. Technol.* **5**, 3411–3416 (2014).
32. S. Frunza, H. Kosslick, A. Schonhals, L. Frunza, I. Enache, T. Beica, *J. Non-Cryst. Solids* **325**,103–112 (2003).
33. Y. Cherifi, A. Chaouchi, Ya. Lorgoilloux, M. Rguiti, Ya. Kadri, C. Courtois, *Process. Appl. Ceram.* **10**,125–135 (2016).
34. R. O Ndong, H. E. Obame, Z. H. Moussambi, N. Koumba, *J. Theor. Appl. Phys.* **12**, 309–317 (2018).
35. P. K. Tripathi, A. K. Misra, K. K. Pandey, R. Manohar, *Chem. Rapid Commun.* **1**, 20-31(2013)